Magnetic Resonance Materials in Physics, Biology and Medicine (2022) 35:533–547
https://doi.org/10.1007/s10334-021-00957-6

REVIEW

Diffusion-weighted imaging in prostate cancer

Tsutomu Tamada[1] · Yu Ueda[2] · Yoshiko Ueno[3] · Yuichi Kojima[1] · Ayumu Kido[1] · Akira Yamamoto[1]

Received: 5 July 2021 / Revised: 11 August 2021 / Accepted: 29 August 2021 / Published online: 7 September 2021

Abstract
Diffusion-weighted imaging (DWI), a key component in multiparametric MRI (mpMRI), is useful for tumor detection and localization in clinically significant prostate cancer (csPCa). The Prostate Imaging Reporting and Data System versions 2 and 2.1 (PI-RADS v2 and PI-RADS v2.1) emphasize the role of DWI in determining PIRADS Assessment Category in each of the transition and peripheral zones. In addition, several recent studies have demonstrated comparable performance of abbreviated biparametric MRI (bpMRI), which incorporates only T2-weighted imaging and DWI, compared with mpMRI with dynamic contrast-enhanced MRI. Therefore, further optimization of DWI is essential to achieve clinical application of bpMRI for efficient detection of csPC in patients with elevated PSA levels. Although DWI acquisition is routinely performed using single-shot echo-planar imaging, this method suffers from such as susceptibility artifact and anatomic distortion, which remain to be solved. In this review article, we will outline existing problems in standard DWI using the single-shot echo-planar imaging sequence; discuss solutions that employ newly developed imaging techniques, state-of-the-art technologies, and sequences in DWI; and evaluate the current status of quantitative DWI for assessment of tumor aggressiveness in PC.

Keywords Prostate neoplasms · MRI · Diffusion-weighted imaging

Introduction

It has been estimated that about 248,530 new cases of prostate cancer (PCa) will be diagnosed in the United States during 2021, and this disease is the second-leading cause of cancer death for men in most Western countries [1, 2]. Accordingly, early detection of PCa with accurate assessment of tumor aggressiveness and local staging is essential to improve mortality rates as well as patient prognosis. Multiparametric MRI (mpMRI) comprising T2-weighted imaging (T2WI), diffusion-weighted imaging (DWI), and dynamic contrast-enhanced MRI (DCE-MRI) prior to prostate biopsy, followed by MR-guided prostate biopsy (such as MRI–ultrasound fusion-guided prostate biopsy), is the recommended protocol to replace standard systematic prostate biopsy for detection of PCa in patients with elevated PSA levels [3–6]. mpMRI, especially DWI, has already made a strong contribution to the accumulation of research results with regard to the detection and localization of primary clinically significant PCa (csPCa) and local recurrence, assessment of tumor aggressiveness by such as Gleason score (GS) and Gleason grade (GG), local staging, active surveillance (AS), and standardization of prostate MRI diagnosis [the Prostate Imaging Reporting and Data System version (PI-RADS)] [7–21]. Furthermore, in recent years, numerous studies regarding biparametric MRI (bpMRI), which does not include DCE-MRI, have reported comparable diagnostic accuracy between bpMRI and mpMRI for detecting csPCa [22–28]. Therefore, the role of DWI in csPCa detection is becoming increasingly important, and its optimization is an urgent issue. In this review article, we discuss the problems of standard DWI with single-shot echo-planar imaging (ssEPI) and their countermeasures, as well as the possibility of clinical application of quantitative DWI, and the latest DWI technology.

✉ Tsutomu Tamada
ttamada@med.kawasaki-m.ac.jp

[1] Department of Radiology, Kawasaki Medical School, 577 Matsushima, Kurashiki city, Okayama 701-0192, Japan

[2] Philips Japan, Konan 2-13-37, Minato-ku, Tokyo, Japan

[3] Department of Radiology, Kobe University Graduate School of Medicine, Kobe, Japan

New technology to overcome problems in standard DWI

Susceptibility artifact and geometric anatomic distortion

Currently, clinical DWI acquisition is routinely performed using two-dimensional (2D) ssEPI technique. DWI with 2D ssEPI (ssEPI DWI) has high signal-to-noise ratio (SNR) and is minimally affected by motion artifact due to its rapid acquisition. However, the image quality of ssEPI DWI suffers from susceptibility artifact caused by gas within the adjacent rectum and by hip implants, and from marked geometric anatomical distortion resulting from factors such as the very rapid acquisition, B0- and B1-field inhomogeneities, and eddy currents [29, 30]. These effects become more pronounced at higher field strength of 3T, which is widely used in prostate mpMRI. Therefore, we need to continue to verify the usefulness of bowel preparation techniques and develop MRI techniques that can improve image quality.

The basic countermeasures against susceptibility artifact and geometric anatomical distortion in ssEPI DWI include dietary restrictions and administration of hyoscine *N*-butylbromide to reduce intestinal peristalsis before the MRI examination. Schmidt et al. have reported that among hyoscine *N*-butylbromide, microenema, and dietary restrictions for artifact reduction and image quality in prostate mpMRI, only microenema appeared to significantly improve the image quality of DWI and the whole mpMRI image set of the prostate [31]. A review article that compared the effectiveness of antispasmodics and rectal enemas concluded that intravenous hyoscine butylbromide was the optimum patient preparation method for improving T2W and DWI image quality in prostate mpMRI, and did not recommend the use of a preparatory rectal enema [32]. Therefore, it is necessary to take active measures to improve image quality of ssEPI DWI using MRI techniques while continuing to verify the clinical usefulness of bowel preparation techniques.

Turbo spin-echo DWI (TSE DWI)

SsTSE DWI combines TSE readout with a single-shot acquisition. TSE readout is not sensitive to susceptibility artifact, whereas single-shot acquisition can shorten the scan time and is not sensitive to motion effect. Initially, signal loss and artifact were drawbacks of ssTSE DWI, because the refocusing pulses after DW preparation violate the Carr–Purcell–Meiboom–Gill (CPMG) condition. Imperfect 180° refocusing of RF pulses will generate both spin echoes (SEs) and stimulated echoes (STEs). If the signal phase after the excitation RF pulse aligns with the phase of subsequent refocusing pulses, STE does not occur. However, as spins are left with unpredictable magnetization phases after DW preparation and this condition is significantly worsened by the presence of tissue motion during DW preparation, STEs are generated. Therefore, the combination of imperfect refocusing RF pulses and random signal phase after DW preparation leads to destructive interference between SEs and STEs, inconsistent signal losses, and consequent image artifacts. Alsop proposed a method that applies a 90° pulse, dephasing gradient, and rephrasing gradient to eliminate non-CPMG (i.e., STE) components [33]. The CPMG condition, which requires alignment of the initial transverse magnetization with the axis of the refocusing pulses, is violated due to random phase error accumulated during the diffusion preparation, which is termed non-CPMG condition. The non-CPMG component of the signal is effectively "hidden" along the longitudinal axis by a 90° pulse prior to the echo train. Because the non-CPMG component that causes artifacts is not acquired, SNR is reduced.

Split acquisition of fast spin-echo signals for diffusion imaging (SPLICE) [34] has been developed to overcome low SNR in ssTSE DWI. This sequence acquires the SE and STE components separately using unbalanced readout gradient and then reconstructs each k-space separately to avoid destructive phase interference. SPLICE with high SNR could be a new option against severe distortion. Figure 1 shows a clinical case in which prostate imaging was obtained using ssEPI DWI, ssTSE DWI, and SPLICE.

Reduced field-of-view DWI

A recently introduced technology for EPI acquisition termed "reduced field-of-view" (rFOV)-DWI has potential for improving image quality, including issues associated with standard ssEPI DWI such as anatomic distortion and susceptibility artifact. rFOV-DWI can be acquired using commercially available sequences such as ZOOM DWI (Philips), ZOOMit (Siemens), and FOCUS (GE), and employs 2D spatially selective excitation pulses instead of the 1D excitation pulse of standard EPI DWI; therefore, it allows excitation of only a small inner volume along the phase-encoding direction and reduces the number of phase-encoding steps [35–37]. This 2D excitation prolongs the time required for the initial radiofrequency pulse. However, the more recent use of parallel transmission (pTx) with independent radiofrequency transmitter channels enables acceleration of the 2D spatially selective excitation pulse, thus improving the practicality of rFOV-DWI within clinical protocols [38, 39]. Several clinical studies have already investigated the impact of rFOV-DWI for optimizing prostate imaging [36,

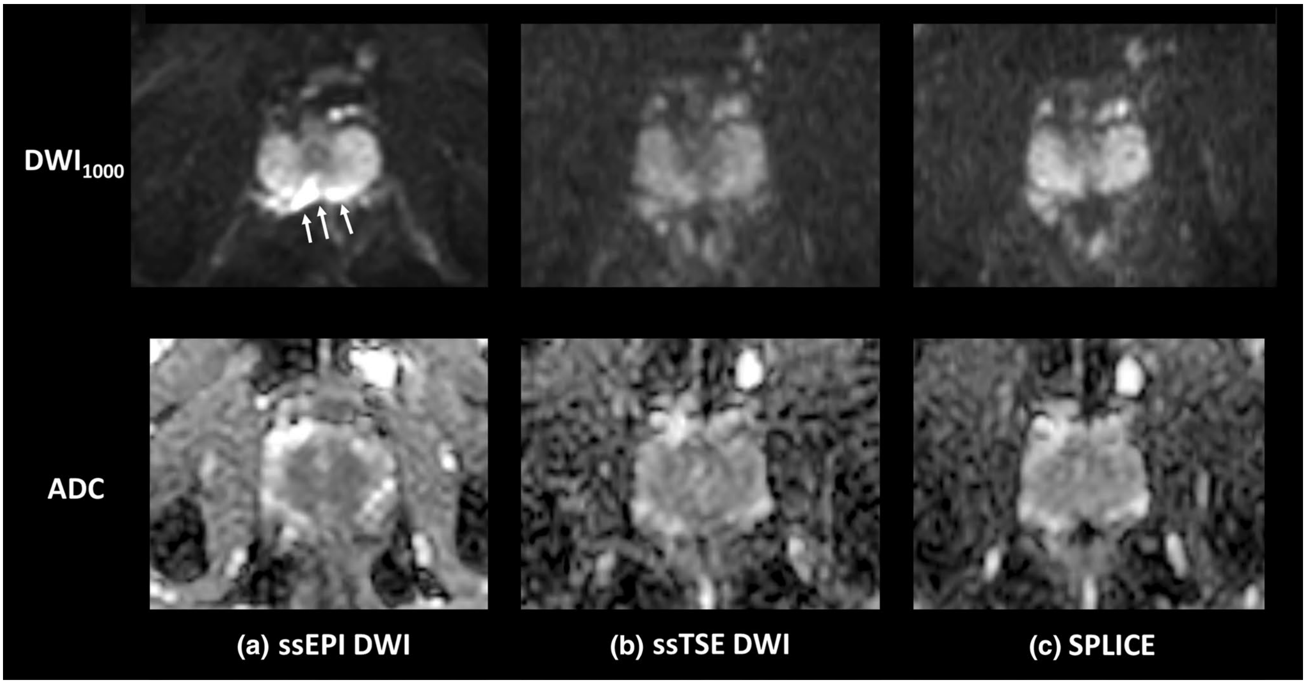

Fig. 1 A 40-year-old male without prostate cancer. ssEPI DWI image (**a**) shows distortion of the prostate due to air in the rectum. In comparison, ssTSE DWI (**b**) and SPLICE (**c**) are less affected by such distortion. Note the higher signal-to-noise ratio of the prostate with SPLICE (**c**) than with ssTSE DWI (**b**). *ssEPI* single-shot echo-planar imaging, *DWI* diffusion-weighted imaging, *ssTSE* single-shot turbo spin-echo; SPLICE, split acquisition of fast spin-echo signals for diffusion imaging

37, 40–44]. These studies have reported substantial improvement in image quality with rFOV-DWI, including reduced anatomical distortion and artifacts. However, two previous studies (using b values of 50 and 800–1000 s/mm^2 and FOV of 104×64 mm^2 and 88×148 mm^2) that assessed tumor detection in PCa reported no improvement in diagnostic performance for rFOV-DWI compared with standard DWI [36, 44]. Tamada et al. considered that the lack of improvement in tumor detection ability using rFOV-DWI may be related to the lower SNR of rFOV-DWI, and the impact of this lower SNR on image contrast such as contrast-to-noise ratio (CNR), if the acquisition time of rFOV-DWI is the almost the same as that of standard DWI [36, 37]. Therefore, further technical optimization of the acquisition method is required to improve SNR and image contrast and thus stabilize image quality in rFOV-DWI. Hausmann et al. has reported that reduced FOV in high b value DWI (b value of 2000 s/mm^2) in combination with T2WI could be useful for detecting csPCa [45].

Blurring

Another drawback in ssEPI DWI is blurring due to T2* attenuation, which shows an increasing tendency at higher field strengths [46–48]. Although parallel imaging enables a dramatic reduction in blurring [49, 50], it remains a problem in ssEPI DWI, especially in high-resolution images.

DWI with multishot EPI

Multi-shot EPI (msEPI) DWI, in which k-space data are acquired in multiple excitations, can reduce blurring due to shorter shot length, but is sensitive to motion caused by phase differences between shots [51, 52]. msEPI DWI can be acquired using commercially available sequences such as image reconstruction using the image-space sampling function (IRIS) in Philips, read-out-segmented EPI multi-shot (RESOLVE) in Siemens, and multiplexed sensitivity encoding (MUSE) in GE [52–54]. In msEPI DWI, multiple excitation is performed in the phase direction for IRIS and MUSE and in the frequency direction for RESOLVE. Regarding the application of msEPI DWI to prostate imaging, a recent study at 3T has reported that subjective image quality taking into account artifacts, delineation of anatomic structures and borders, overall sharpness, contrast, and overall subjective impression; and CNR of PCa and benign tissue, were all higher for msEPI DWI than for ssEPI DWI, but that SNR was lower for msEPI DWI than for ssEPI DWI [55] (Fig. 2). Because distortion and blurring are reduced in msEPI DWI compared with ssEPI DWI, we would expect msEPI DWI to contribute to improved diagnostic performance in local

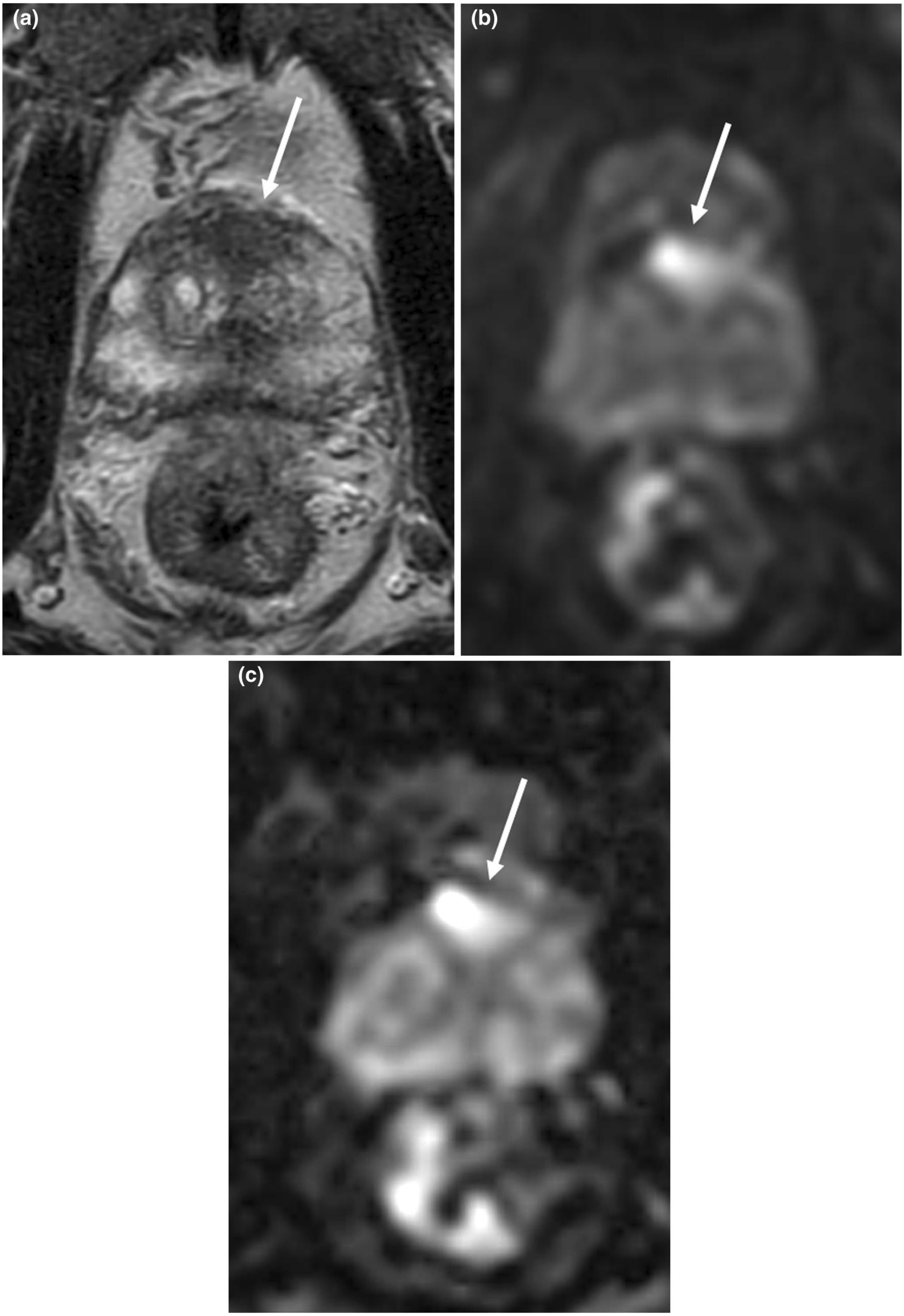
(a)
(b)
(c)

◂**Fig. 2** An 80-year-old male with prostate cancer (PSA level, 13.69 ng/mL; Gleason score, 3 + 4) in the transitional zone. A homogeneous hypointense lesion is seen on T2-weighted imaging (**a**) (arrow). A focal hyperintensity is depicted clearly on ssEPI DWI (**b**) and msEPI DWI (**c**) (arrow) DWI. SNR is higher in ssEPI DWI (**b**) than msEPI DWI (**c**), whereas sharpness is better in msEPI DWI (**c**) than ssEPI DWI (**b**). CNR between prostate cancer and benign prostate is comparable between the two DWI sequences (**b** and **c**). *PSA* prostate-specific antigen, *DWI* diffusion-weighted imaging, *ssEPI* single-shot echo-planar imaging, *msEPI* multi-shot echo-planar imaging, *SNR* signal-to-noise ratio, *CNR* contrast-to-noise ratio

staging for such as extracapsular extension (Fig. 3). However, acquisition time is much longer in msEPI DWI than in ssEPI DWI, which must be improved before msEPI DWI can be applied for clinical prostate MRI.

Image contrast between benign and malignant tissues

Ultra-high *b* value DWI (uhDWI)

In prostate mpMRI, high *b* value DWI (hDWI) with *b* values of 1500–2000 s/mm^2 is commonly used in daily clinical practice [20, 21]. However, even hDWI shows insufficient image contrast between benign and malignant tissues. Therefore, it would be useful to determine whether higher *b* value DWI could improve the clinical performance of PCa detection. As one possible solution, computed DWI obtained as a calculation image using standard *b* values such as 800–1000 s/mm^2 may be useful for improving the image contrast [20, 21, 56]. A study that used a wide range of computed *b* values (1000–5000 s/mm^2) has demonstrated that those in the range of 1500–2500 s/mm^2 are optimal for PCa detection; and that computed *b* values of 1000 and 3000–5000 s/mm^2 exhibit lower performance related to insufficient signal suppression at the low *b* value and excessive signal suppression leading to diminished anatomic clarity at the higher *b* values, respectively [57]. A recent study showed that PCa detection rates in computed DWIs with *b* values of 2000 and 2500 s/mm^2 were similar to that of native-acquired DWI with *b* value of 2000 s/mm^2 [58]. Vural et al. showed that lesion detection rates were the same for computed *b* values of 2000 and 3000 s/mm^2, both of which were better than for a computed *b* value of 1500 s/mm^2 [59]. Therefore, the clinical application of computed uhDWI with high *b* value such as 3000 s/mm^2 may not be realistic for improving PCa detection ability. In addition, computed DWI requires dedicated post-processing software as well as extra post-processing time. As a second solution in the acquisition of higher *b* value DWI that may have potential for the clinical application of uhDWI, improvement in SNR may be gained by state-of-the-art 3T MRI with extremely high gradient waveform fidelity (≈100%), achieved by improved eddy current calibration with maximum gradient strength and maximum slew rate due to precisely calculated coil design and high cooling efficiency. In the study of Zang et al. that evaluated the efficacy of native-acquired uhDWI for PCa detection, native-acquired uhDWI with a *b* value of 3000 s/mm^2 had higher area under the curve (AUC) for PCa tumor detection compared with native-acquired DWIs with *b* values of 1000 and 2000 s/mm^2 [60] (Fig. 4). Thus, such diagnostic performance of uhDWI for PCa detection should be further confirmed in prospective multi-institutional clinical trials with a larger number of patients.

Quantitative DWI for assessment of tumor aggressiveness in PCa

Clinical impact of accurate assessment of tumor aggressiveness in PCa

PCa can be classified as csPCa, for which curative therapies such as radical prostatectomy are indicated, or as clinically insignificant PCa (cisPCa), for which AS using serum prostate-specific antigen (PSA) is indicated. Therefore, accurate pre-treatment risk stratification of PCa is essential in determining the treatment strategy. In general, csPCa is defined based on histopathology as Gleason score (GS) ≥ 3 + 4, and/or tumor volume ≥ 0.5 cc, and/or extracapsular extension [20]. Among these determining elements of pre-treatment risk stratification in PCa, a tumor GS that reflects tumor aggressiveness would be strongly associated with signal intensity change on DWI and ADC map, as in the DWI scoring system in PI-RADS v2.1 [21] (Table 1). Systematic ultrasonography-guided prostate biopsy, which is a standard method for histopathological evaluation of PCa before treatment in patients with elevated PSA levels has several limitations, including underestimation of indicators of tumor aggressiveness such as the GS of PCa [61, 62]. Therefore, clinical study using quantitative parameters of DWI such as ADC is being actively performed to discriminate PCa aggressiveness.

DWI with standard mono-exponential model

DWI reflects the Brownian movement of water molecules mainly within extracellular space and is influenced by changes in the relative volumes of glandular, epithelial, and stromal components, as occurs in malignancy [63, 64]. DWI is a key method for tumor detection in prostate mpMRI and also for assessment of tumor aggressiveness in patients with PCa [9, 65]. Previous studies that have employed ADC calculated using a mono-exponential model from DWI acquisitions could discriminate between low-risk and moderate-to-high-risk PCa [9]. However, because there is much

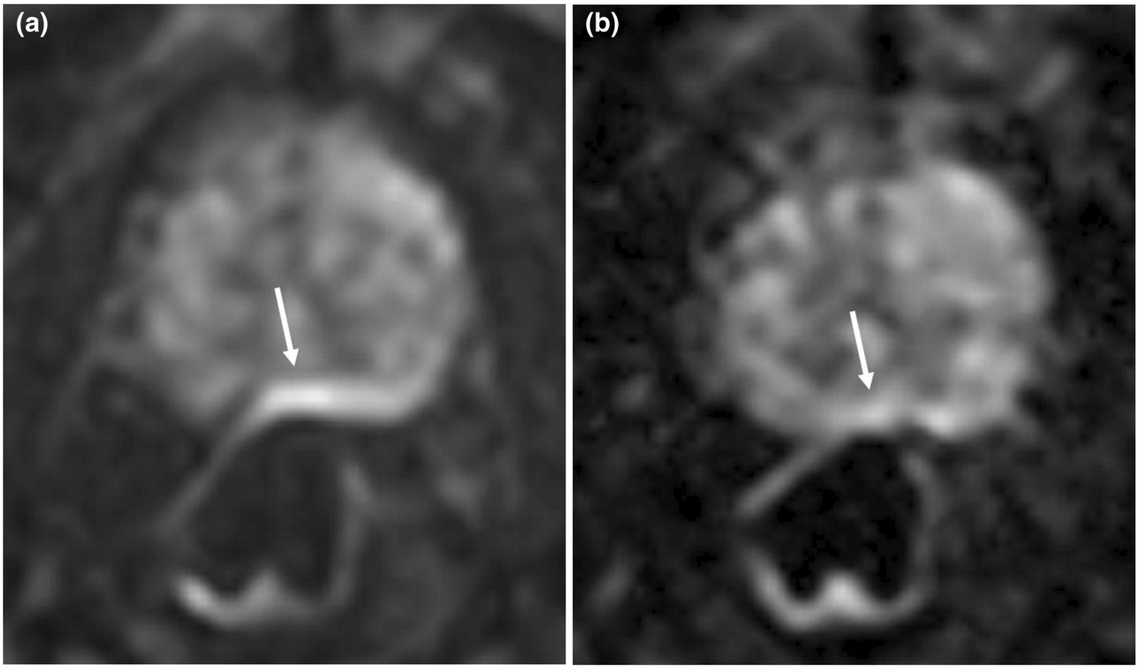

Fig. 3 An 83-year-old male with prostate cancer (PSA level, 6.6 ng/mL; Gleason score, 3 + 4) in the peripheral zone. No lesion is apparent on ssEPI DWI (**a**) or msEPI DWI (**b**), both of which show distortion of the prostate due to rectal air. msEPI DWI (**b**) is less affected by distortion induced by rectal gas compared with ssEPI DWI (**a**). *PSA* prostate-specific antigen, *DWI* diffusion-weighted imaging, *msEPI* multi-shot echo-planar imaging, *ssEPI* single-shot echo-planar imaging

overlap between the ADC values of low- and high-grade tumors [66–70], further optimization of DWI methodology is needed to improve the diagnostic performance of diffusion measurements.

The ADC computation assumes Gaussian behavior of water diffusion, whereby water molecules are treated as moving freely and a simple mono-exponential fitting model is applied to characterize the signal decay (Fig. 5). ADC is calculated for a pair of b values (e.g., 0 and 1000 s/mm^2) using the following equation:

$Sb = S0 \cdot \exp\{-b \cdot ADC\}$.

ADC histogram analysis

ADC histogram analysis is noteworthy as a measure for improving the diagnostic performance of standard ADC, and includes metrics such as the mean, median, various percentile values, skewness as a measure of the asymmetry of the distribution, entropy as a measure of the randomness of the distribution, and kurtosis as a measure of the sharpness of the peak of the distribution [16]. ADC parameters such as the 10th percentile derived from ADC histogram analysis have been found to have higher discrimination ability for tumor aggressiveness compared with the mean ADC value [71, 72]. Lower tumor ADC regions such as the 10th percentile of ADC derived from the ADC histogram analysis may be related to its sensitivity to more aggressive sub-regions within a heterogeneous tumor in PCa [71, 73] that might not be appreciated using conventional metrics such as mean value by volume averaging. A study by Tamada et al. using PCa patients under AS have reported that the mean 0–10th percentile value of 3D whole-lesion ADC histogram analysis in the baseline MRI examination had the best performance for predicting lesion growth on serial MRI examinations, and the change in lesion volume on serial examinations was associated with tumor aggressiveness on follow-up targeted biopsy [16]. Furthermore, histogram analysis can be applied to various other Gaussian and non-Gaussian fitting models as well as to standard ADC. ADC histogram analysis has recently been performed using a simple region of interest (ROI) placement technique on standard Picture Archiving and Communication System (PACS), without using dedicated software such as non-Gaussian fitting models.

Bi-exponential model and non-Gaussian fitting model

It is considered that because water molecule diffusion is obstructed by microstructural complexity (including cellular membranes) in PCa tissues, more complex Gaussian and non-Gaussian models may better reflect the diffusion behavior in PCa, which is characterized by tissue heterogeneity within the tumor [74]. The bi-exponential and non-Gaussian fitting models for which there are abundant

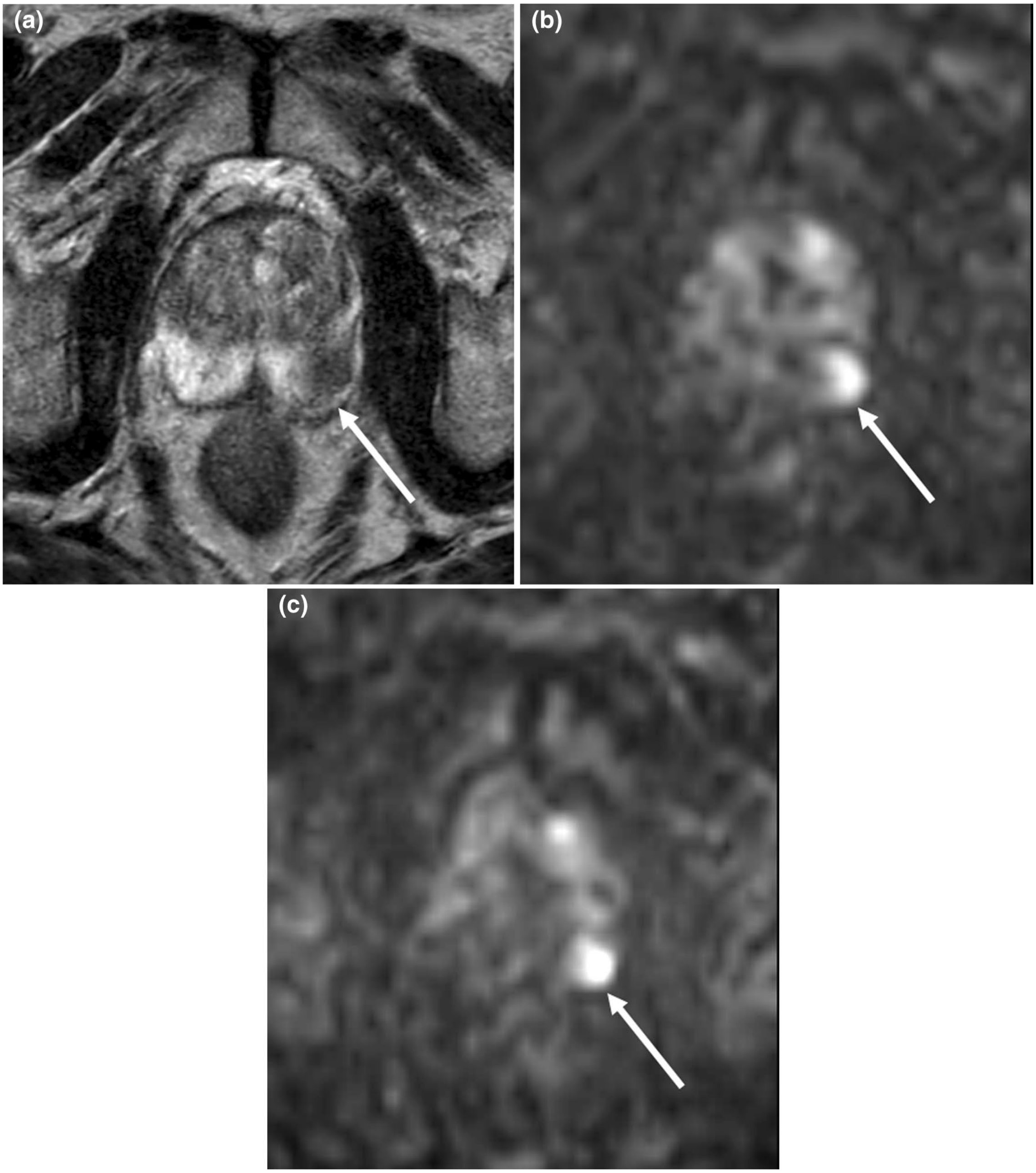

Fig. 4 A 79-year-old male with prostate cancer (PSA level, 8.01 ng/mL; Gleason score, 4 + 3) in the posterior left region of the peripheral zone. A homogeneous hypointense lesion with mass effect is seen on T2-weighted imaging (**a**) (arrow). Signal intensity of the benign whole prostate is lower in DWI with *b* values of 0 and 3000 s/mm^2 (**c**) than in DWI with *b* values of 0 and 2000 s/mm^2 (**b**). The lesion is depicted clearly as a focal hyperintensity (arrows) in DWI with *b* values of 0 and 3000 s/mm^2 (**c**), compared with DWI with *b* values of 0 and 2000 s/mm^2 (**b**). *PSA* prostate-specific antigen, *DWI* diffusion-weighted imaging

research results mainly include intravoxel incoherent motion (IVIM), stretched exponential model, and diffusion kurtosis imaging (DKI).

The bi-exponential fitting and non-Gaussian behavior of diffusion can be investigated using DWI with high *b* values and with a relatively large number of *b* values, following recent advances in hardware and software that have enabled the use of higher *b* values such as 2000 s/mm^2 and advanced DWI acquisition and modeling methods [75]. In IVIM and the stretched exponential model, it is desirable to use a large number of *b* values ranging from very low to high, which might be a more reliable and reproducible method for assessing tumor aggressiveness compared with the mono-exponential model [76–78].

Table 1 Scoring system of diffusion-weighted imaging for assessment of transition zone and peripheral zone in PI-RADS v2.1

Score	PI-RADS v2.1
1	No abnormality (i.e., normal) on ADC map and DWI
2	Linear/wedge-shaped hypointense on ADC and/or linear/wedge-shaped hyperintense on high *b* value DWI
3	Focal (discrete and different from the background) hypointense on ADC and/or focal hyperintense on high *b* value DWI; may be markedly hypointense on ADC or markedly hyperintense on high *b* value DWI, but not both
4	Focal markedly hypointense on ADC and markedly hyperintense on high *b* value DWI; < 1.5 cm in greatest dimension
5	Same as 4 but ≥ 1.5 cm in greatest dimension or definite extraprostatic extension/invasive behavior

PI-RADS Prostate Imaging Reporting and Data System, *ADC* apparent diffusion coefficient, *DWI* diffusion-weighted imaging

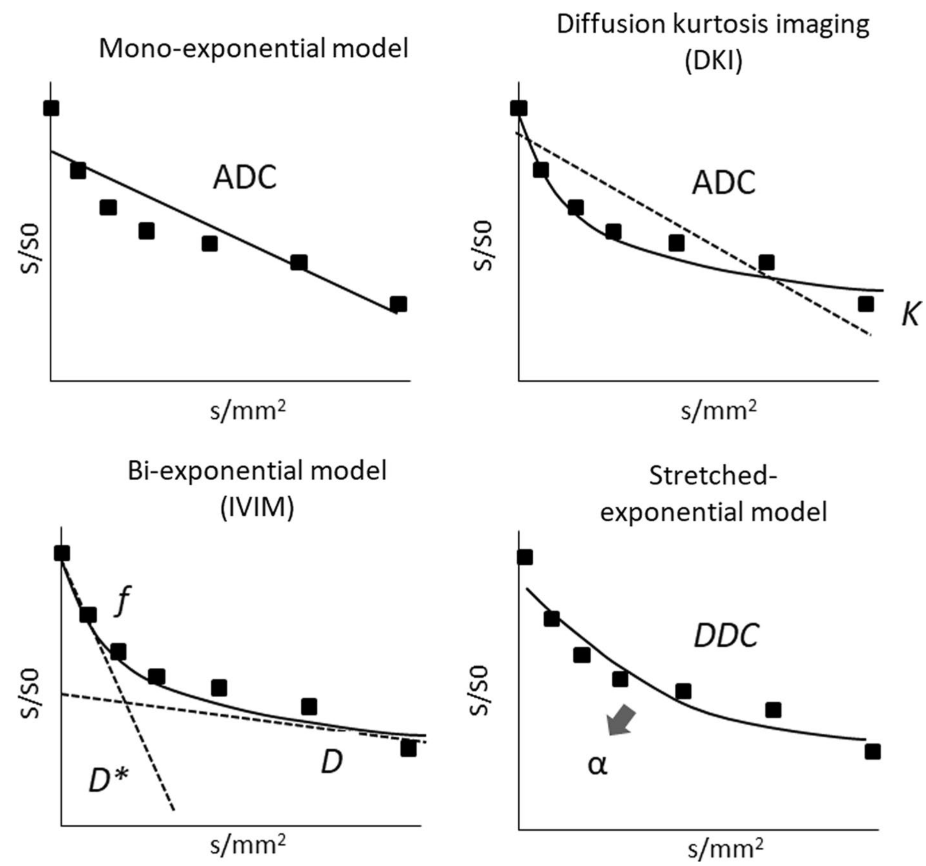

Fig. 5 Mathematical models employed in diffusion-weighted imaging. ADC, apparent diffusion coefficient; *K*, diffusional kurtosis; IVIM, intravoxel incoherent motion; *f*, perfusion fraction; D^*, perfusion-related diffusion coefficient, *D*, molecular diffusion coefficient, α, stretching parameter; *DDC*, distributed diffusion coefficient

IVIM

IVIM is a bi-exponential fitting model that separately evaluates extravascular molecular diffusion and microcirculation of blood within the capillaries [76, 77] (Fig. 5). It is calculated using bi-exponential fitting with multiple *b*-values, with the following equation:

$$S_b = S_0\{F \bullet \exp(-bD^*) + (1 - F) \bullet \exp(-bD)\}$$

where D^* and F are the perfusion-related diffusion coefficient and microvascular volume fraction, respectively; and D is the molecular diffusion coefficient.

Numerous previous investigations of IVIM DWI have reported comparable diagnostic performance of PCa risk stratification between IVIM (mainly *D*) and mono-exponential model ADC [70, 79–84], whereas only one study has observed better performance of *D* in IVIM compared with mono-exponential model ADC [85]. Among these studies, two assessed IVIM DWI using *b* values of 2000 s/mm^2 or higher [80, 84]. In contrast, many previous studies have shown insufficient diagnostic performance of *f* in IVIM [70, 81, 83, 85].

Stretched exponential model

The stretched exponential model reflects the deviation of the curve from mono-exponential behavior (Fig. 5). It is performed with multiple *b* values, using the following equation:

$$S_b = S_0 \bullet \exp\{-(bDDC)^{\alpha}\}$$

where *DDC* is the distributed diffusion coefficient, which shows the rate of signal decay with increasing *b* values; and α is the stretching parameter, which characterizes the deviation of the signal attenuation from the mono-exponential model. A value close to one indicates high homogeneity in apparent diffusion, whereas a low-value result from the non-exponential model is caused by the addition of multiple components.

The diagnostic performance of the stretched exponential model (mainly *DDC*) for risk stratification of PCa tends to be similar to that of mono-exponential ADC [78, 86, 87]. These studies regarding the stretched exponential model were performed using high *b* value DWI with multiple *b* values such as 1500 s/mm^2 or higher [78, 86, 87]. Several investigators have reported that the similar diagnostic capabilities for assessment of tumor aggressiveness among mono-exponential ADC, IVIM, and the stretched exponential model may be due to strong correlations between these models, or between GS and these models, which may suggest that these models individually provide similar information in PCa [78, 80–82, 86].

DKI

DKI is a non-Gaussian DWI fitting model that is believed to better reflect the microstructural complexity of biologic tissue compared with mono-exponential ADC [88]. Like IVIM and the stretched exponential model, DKI also requires higher *b* values during acquisition, such as 2,000 s/mm^2, and quantifies the deviation of tissue diffusion from a Gaussian pattern as diffusional kurtosis (*K*) [89] (Fig. 5). An elevation in *K* indicates greater tissue complexity and deviation from Gaussian behavior, and the *K* value has been reported to be higher in various malignant tumors than in normal tissues. DKI is calculated with multiple *b* values, using the following equation:

$$S = S0 \cdot \exp\left(-\mathrm{b} \cdot D + \mathrm{b}^2 \cdot D^2 \cdot K/6\right) \tag{1}$$

where *K* has no units and represents excess kurtosis relative to a mono-exponential fitting, being 0 for perfectly Gaussian diffusion, and increasing for greater deviation from the Gaussian pattern; and *D* is an analog of ADC that is adjusted for non-Gaussian diffusion behavior.

Among numerous studies with relatively small sample size that have compared mono-exponential ADC and DKI for assessing PCa aggressiveness [78, 88–93], some have observed better performance of either DKI or mono-exponential ADC [88–90, 93], whereas others have reported similar diagnostic performance [78, 91, 92]. A previous large study at 3 T that included 285 PCa patients compared the discrimination ability of PCa tumor aggressiveness using radical prostatectomy as reference standard between mono-exponential ADC (with three *b* values of 0, 500, and 1000 s/mm^2) and DKI (with five *b* values of 0, 500, 1000, 1500, and 2000 s/mm^2) for characterization of PCa [74]. ADC and *K* were highly correlated ($r = -0.82$), with similar diagnostic performance for GS $\leq 3+3$ tumors vs. GS $\geq 3+4$ tumors (AUC 0.744 for ADC and 0.715 for *K*) and for GS $\leq 3+4$ tumors vs. GS $\geq 4+3$ tumors (AUC 0.720 for ADC and 0.694 for *K*) [75]. In addition, a recent DWI study that used 11 *b* values (0, 50, 100, 200, 900, 1100, 1400, 1800, 2200, 2500, and 3000 s/mm^2) at 3T has reported diagnostic performance of the IVIM and DKI models comparable to that of mono-exponential ADC for prediction of PCa tumor aggressiveness (GS $\leq 3+4$ tumors vs. GS $\geq 4+3$ tumors; AUC 0.744 for ADC, 0.732 for *D*, and 0.766 for *K*) [80]. Therefore, these metrics appear to be providing, to some extent, overlapping information for the measures of diffusivity and kurtosis [74, 88, 90]. Furthermore, it should be noted that analysis with the non-Gaussian fitting models requires dedicated post-processing software and longer post-processing time than that required for mono-exponential ADC.

Thus, at the present time, it can be considered that no non-Gaussian and bi-exponential fitting models have diagnostic capabilities that clearly outperform mono-exponential ADC. In the clinical setting, the use of simple mono-exponential ADC with histogram analysis may be appropriate for assessing PCa tumor aggressiveness. In addition, recent investigations have reported the potential of mpMRI including mono-exponential ADC-based radiomics models, as a machine-aided approach, for predicting PCa aggressiveness [94–96].

Microstructural MRI

An advanced imaging technique based on DWI for mpMRI-invisible csPCa

Although mpMRI is a well-established imaging method that is widely used in conjunction with a standardized reading method (PI-RADS) in prostate imaging, a certain percentage of csPCas are missed as mpMRI-invisible tumors [97–100]. To address this unmet clinical need, microstructural MRI has been newly developed as a quantitative technique that focuses on structural change in three typical microstructures of prostatic tissue: epithelial cells, stroma, and glandular lumen [101]. Diffusion-based microstructural MRI includes restriction spectrum imaging (RSI), Vascular, Extracellular and Restricted Diffusion for Cytometry in Tumors (VERDICT), hybrid multidimensional MRI (HM MRI), and diffusion-time dependent diffusion MRI (dMRI) using oscillating and pulsed gradient spin-echo sequences (OGSE) [102, 103]. A summary of these diffusion-based microstructural MRI methods is provided in Table 2 (Fig. 6).

RSI

RSI is a novel diffusion-based technique initially developed for neuroimaging. It uses the data obtained from a broad range of multiple *b* values obtained in multi-directional diffusion images to model a distribution or a spectrum of isotropic and anisotropic water compartments in tissue [104, 105]. This method might possibly enable isolation of signal from intracellular restricted water, and simultaneously minimize signals from extracellular hindered and free water, which currently hinders conventional DWI [106]. Therefore, as an indicator of signal arising primarily from intracellular water (in other words, cellular components) RSI highlights highly cellular tumors [102]. In a recent study that included a large number of patients with suspected PCa, comparable PCa detection ability was found for RSI and conventional DWI; however, RSI had superior specificity for transition zone (TZ) lesions [107]. Such improvement in diagnostic specificity for TZ lesions by RSI could contribute

Table 2 Diffusion-based microstructural imaging

Sequence	Imaging technique	Target microstructural component	Characterization in PCa
RSI	Multi-directional diffusion-based imaging technique	Cellular component	Highly cellular index
VERDICT	Diffusion-based imaging technique with a mathematical model	Microvascular, extracellular-extravascular and intracellular space	Increased intracellular and microvascular volume and decreased extracellular-extravascular volume
HM MRI	Combination of both diffusion and T2-relaxation technique	Stroma, epithelium, and lumen	Increased epithelium volume and decreased lumen and stroma fractional volume
dMRI using OGSE	Diffusion-based imaging technique, extremely shortened diffusion time	Various indices such as intracellular fraction and cellularity	Increase of intracellular fraction and cellularity with increased GS

RSI restriction spectrum imaging, *VERDICT* Vascular, Extracellular and Restricted Diffusion for Cytometry in Tumors, *HM MRI* hybrid multidimensional MRI, *dMRI* diffusion-time dependent diffusion MRI, *OGSE* oscillating and pulsed gradient spin-echo sequences, *PCa* prostate cancer, *GS* Gleason score

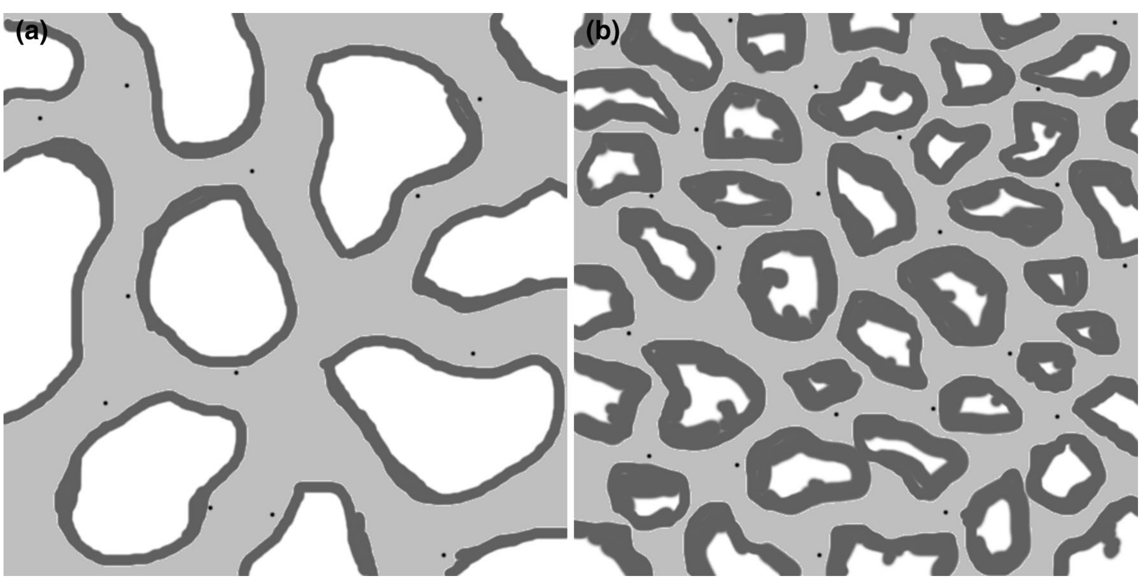

Fig. 6 Representation of prostate histopathology in benign tissue (**a**) and prostate cancer (**b**). Microstructural MRI focuses on change in four types of prostatic microstructure, represented here as follows: epithelial cells (dark gray areas), stroma (gray area), glandular lumen (white areas), and microvasculature (small black circles)

to prediction of csPCa in PI-RADS category 3 equivocal lesions, which are associated with a low detection rate of csPCa in the TZ [28, 108].

VERDICT

VERDICT is a diffusion-based imaging technique that combines a DWI acquisition with a mathematical model and assigns the diffusion signal to three separate water compartments: microvascular, extracellular–extravascular, and intracellular space [101, 109]. PCa is typically characterized by an increase in the volume of intracellular and microvascular space and a decrease in the volume of extracellular–extravascular space [102]. In a study of 70 patients with suspected PCa or undergoing AC, intracellular volume fraction obtained from VERDICT MRI using b values of 90, 500, 1500, 2000, and 3000 s/mm^2 (total imaging time, 12 min 25 s) had a higher AUC for discriminating PCa with a Gleason 4 component from benign tissue and/or PCa with GS = 3 + 3 compared with ADC obtained with standard ADC using b values of 90, 500, 1500, 2000, and 3000 s/mm^2 (total imaging time, 5 min 16 s) (AUC 0.93 vs. 0.85, respectively) [110].

HM MRI

Previous studies have shown that T2 and ADC are strongly interdependent, and that distinct populations of water molecules in each voxel with specific paired T2 and ADC values can be identified [104, 105]. HM MRI measures change in ADC and T2 as a function of echo time (TE) and b value, respectively, and uses these changes as a source of information about underlying tissue microstructure components such as stroma, epithelium, and lumen change [102, 111]. HM MRI is acquired using a spin-echo module with diffusion-sensitizing gradients placed symmetrically about the 180° pulse, followed by ssEPI readout and different combinations of TE and b values (TE of 47, 75, and 100 ms; and b values of 0, 750, and 1500 s/mm^2) (total imaging time, 8–15 min) [102, 111]. Investigation into the use of HM MRI for the prostate is being actively conducted at the University of Chicago [111–113]. In this method, microstructure tissue component volumes are calculated by fitting the HM MRI data to the three-compartment signal model. Distinct paired ADC and T2 values are associated with each compartment, using the following equation:

$$\frac{S}{S_0} = \sum_{n=1}^{n=3} V_n \times \exp\left(-ADC_n \times b - \frac{TE}{T2_n}\right) \quad (2)$$

PCas are characterized by increased epithelium volume and reduced lumen and stroma fractional volumes by HM MRI [111]. In addition, it is noteworthy that correlation coefficients were higher between the fraction volumes of tissue components and tumor GS than between T2 values and tumor GS and between ADCs and tumor GS [113].

Thus, the findings of previous studies indicate that VERDICT MRI and HM MRI are expected to improve characterization in PCa, but that continued technical optimization of these advanced MRI sequences is required to shorten the acquisition time before they can be considered for broader clinical application.

dMRI using OGSE

dMRI using OGSE is a novel DWI technique with extremely shortened diffusion time that enables the calculation of microstructural components such as cellularity in prostate tissue, using a mathematical model. The total acquisition time is around 5 min [103]. A recent preliminary study has demonstrated that intracellular fraction and cellularity obtained from dMRI using OGSE had a positive correlation with GS, and AUC of the cellularity for discriminating between low-grade PCa and intermediate-to-high-grade PCa was 0.964 [103]. Although dMRI using OGSE acquired with a clinically acceptable imaging time is expected to have clinical application for PCa characterization, this method suffers from low spatial resolution, which requires improvement; in addition, it is necessary to verify the association between the microstructural MR findings and the pathological findings.

Conclusion

The role of prostate DWI is continuing to increase in the clinical management of PCa in patients with elevated PSA levels, in such as tumor detection, localization, and characterization. Technological innovations in MRI have led to the proposal of various DWI sequences and post-processing technologies as alternatives to standard ssEPI for optimizing qualitative visual assessment in DWI. Regarding the clinical application of quantitative DWI in the risk stratification of PCa, there appears to be no DWI method with bi-exponential fitting model and non-Gaussian fitting model that outperforms mono-exponential ADC with histogram analysis at the present time. In the future, we can expect state-of-the-art technologies and sequences in DWI, including microstructural MRI, to play a more important role in evaluating csPCa.

Author contributions Drafting of manuscript: TT, YU, YK, and AK. Critical revision: YU, YU, and AY.

Declarations

Conflicts of interest The authors declare that they have no conflict of interest.

Ethical approval This article does not contain any studies with human participants performed by any of the authors.

References

1. American Cancer Society (2021) Cancer facts and figures 2021. American Cancer Society, Atlanta
2. Siegel RL, Miller KD, Fuchs HE, Jemal A (2021) Cancer statistics, 2021. CA Cancer J Clin 71:7–33
3. Ahmed HU, El-Shater Bosaily A, Brown LC, Gabe R, Kaplan R, Parmar MK, Collaco-Moraes Y, Ward K, Hindley RG, Freeman A, Kirkham AP, Oldroyd R, Parker C, Emberton M; PROMIS study group (2017) Diagnostic accuracy of multi-parametric MRI and TRUS biopsy in prostate cancer (PROMIS): a paired validating confirmatory study. Lancet 389:815-822
4. Kasivisvanathan V, Rannikko AS, Borghi M, Panebianco V, Mynderse LA, Vaarala MH, Briganti A, Budäus L, Hellawell G, Hindley RG, Roobol MJ, Eggener S, Ghei M, Villers A, Bladou F, Villeirs GM, Virdi J, Boxler S, Robert G, Singh PB, Venderink W, Hadaschik BA, Ruffion A, Hu JC, Margolis D, Crouzet S, Klotz L, Taneja SS, Pinto P, Gill I, Allen C, Giganti F, Freeman A, Morris S, Punwani S, Williams NR, Brew-Graves C, Deeks J, Takwoingi Y, Emberton M, Moore CM; PRECISION Study Group Collaborators (2018) MRI-Targeted or Standard Biopsy for Prostate-Cancer Diagnosis. N Engl J Med 378:1767-1777
5. Mohler JL, Antonarakis ES, Armstrong AJ, D'Amico AV, Davis BJ, Dorff T, Eastham JA, Enke CA, Farrington TA, Higano CS, Horwitz EM, Hurwitz M, Ippolito JE, Kane CJ, Kuettel MR, Lang JM, McKenney J, Netto G, Penson DF, Plimack ER, Pow-Sang JM, Pugh TJ, Richey S, Roach M, Rosenfeld S, Schaeffer E, Shabsigh A, Small EJ, Spratt DE, Srinivas S, Tward J, Shead DA, Freedman-Cass DA. Prostate Cancer, Version 2.2019, NCCN Clinical Practice Guidelines in Oncology (2019) J Natl Compr Canc Netw 17:479–505
6. Mottet N, van den Bergh RCN, Briers E, Van den Broeck T, Cumberbatch MG, De Santis M, Fanti S, Fossati N, Gandaglia G, Gillessen S, Grivas N, Grummet J, Henry AM, van der Kwast TH, Lam TB, Lardas M, Liew M, Mason MD, Moris L, Oprea-Lager DE, van der Poel HG, Rouvière O, Schoots IG, Tilki D, Wiegel T, Willemse PM, Cornford P. EAU-EANM-ESTRO-ESUR-SIOG Guidelines on prostate cancer-2020 Update. Part 1: screening, diagnosis, and local treatment with curative intent (2021) Eur Urol 2021 79:243–262
7. Schieda N, Lim CS, Zabihollahy F, Abreu-Gomez J, Krishna S, Woo S, Melkus G, Ukwatta E, Turkbey B (2021) Quantitative prostate MRI. J Magn Reson Imaging 53:1632–1645
8. Jie C, Rongbo L, Ping T (2014) The value of diffusion-weighted imaging in the detection of prostate cancer: a meta-analysis. Eur Radiol 24:1929–1941
9. Tamada T, Sone T, Jo Y, Yamamoto A, Ito K (2014) Diffusion-weighted MRI and its role in prostate cancer. NMR Biomed 27:25–38
10. Donati OF, Jung SI, Vargas HA, Gultekin DH, Zheng J, Moskowitz CS, Hricak H, Zelefsky MJ, Akin O (2013) Multiparametric prostate MR imaging with T2-weighted, diffusion-weighted, and dynamic contrast-enhanced sequences: are all pulse sequences necessary to detect locally recurrent prostate cancer after radiation therapy? Radiology 268:440–450
11. Rud E, Baco E, Lien D, Klotz D, Eggesbø HB (2014) Detection of radiorecurrent prostate cancer using diffusion-weighted imaging and targeted biopsies. AJR Am J Roentgenol 202:W241-246
12. Giannarini G, Nguyen DP, Thalmann GN, Thoeny HC (2012) Diffusion-weighted magnetic resonance imaging detects local recurrence after radical prostatectomy: initial experience. Eur Urol 61:616–620
13. Scheenen TW, Rosenkrantz AB, Haider MA, Multiparametric FJJ (2015) Magnetic resonance imaging in prostate cancer management: current status and future perspectives. Invest Radiol 50:594–600
14. Tamada T, Sone T, Kanomata N, Miyaji Y, Kido A, Jo Y, Yamamoto A, Ito K (2016) Value of preoperative 3T multiparametric MRI for surgical margin status in patients with prostate cancer. J Magn Reson Imaging 44:584–593
15. Woo S, Cho JY, Kim SY, Kim SH (2015) Extracapsular extension in prostate cancer: added value of diffusion-weighted MRI in patients with equivocal findings on T2-weighted imaging. AJR Am J Roentgenol 204:W168-175
16. Tamada T, Dani H, Taneja SS, Rosenkrantz AB (2017) The role of whole-lesion apparent diffusion coefficient analysis for predicting outcomes of prostate cancer patients on active surveillance. Abdom Radiol (NY) 42:2340–2345
17. Henderson DR, de Souza NM, Thomas K, Riches SF, Morgan VA, Sohaib SA, Dearnaley DP, Parker CC, van As NJ (2016) Nine-year follow-up for a study of diffusion-weighted magnetic resonance imaging in a prospective prostate cancer active surveillance cohort. Eur Urol 69:1028–1033
18. Kim TH, Jeong JY, Lee SW, Kim CK, Park BK, Sung HH, Jeon HG, Jeong BC, Seo SI, Lee HM, Choi HY, Jeon SS (2015) Diffusion-weighted magnetic resonance imaging for prediction of insignificant prostate cancer in potential candidates for active surveillance. Eur Radiol 25:1786–1792
19. Barentsz JO, Richenberg J, Clements R, Choyke P, Verma S, Villeirs G, Rouviere O, Logager V, Fütterer JJ (2012) European society of urogenital radiology. ESUR prostate MR guidelines Eur Radiol 22:746–757
20. Weinreb JC, Barentsz JO, Choyke PL, Cornud F, Haider MA, Macura KJ, Margolis D, Schnall MD, Shtern F, Tempany CM, Thoeny HC, Verma S (2016) PI-RADS prostate imaging - reporting and data system: 2015, version 2. Eur Urol 69:16–40
21. Turkbey B, Rosenkrantz AB, Haider MA, Padhani AR, Villeirs G, Macura KJ, Tempany CM, Choyke PL, Cornud F, Margolis DJ, Thoeny HC, Verma S, Barentsz J, Weinreb JC (2019) Prostate imaging reporting and data system version 2.1: 2019 update of prostate imaging reporting and data system version 2. Eur Urol 76:340–351
22. Alabousi M, Salameh JP, Gusenbauer K, Samoilov L, Jafri A, Yu H, Alabousi A (2019) Biparametric vs multiparametric prostate magnetic resonance imaging for the detection of prostate cancer in treatment-naïve patients: a diagnostic test accuracy systematic review and meta-analysis. BJU Int 124:209–220
23. Kang Z, Min X, Weinreb J, Li Q, Feng Z, Wang L (2019) Abbreviated biparametric versus standard multiparametric MRI for diagnosis of prostate cancer: a systematic review and meta-analysis. AJR Am J Roentgenol 212:357–365
24. Woo S, Suh CH, Kim SY, Cho JY, Kim SH, Moon MH (2018) Head-to-head comparison between biparametric and multiparametric mri for the diagnosis of prostate cancer: a systematic review and meta-analysis. AJR Am J Roentgenol 211:W226–W241
25. Niu XK, Chen XH, Chen ZF, Chen L, Li J, Peng T (2018) Diagnostic performance of biparametric MRI for detection of prostate cancer: a systematic review and meta-analysis. AJR Am J Roentgenol 211(2):369–378

26. Bass EJ, Pantovic A, Connor M, Gabe R, Padhani AR, Rockall A, Sokhi H, Tam H, Winkler M, Ahmed HU (2020) A systematic review and meta-analysis of the diagnostic accuracy of biparametric prostate MRI for prostate cancer in men at risk. Prostate Cancer Prostatic Dis. https://doi.org/10.1038/s41391-020-00298-w
27. Cuocolo R, Verde F, Ponsiglione A, Romeo V, Petretta M, Imbriaco M, Stanzione A (2021) Clinically significant prostate cancer detection with biparametric MRI: a systematic review and meta-analysis. AJR Am J Roentgenol 216:608–621
28. Tamada T, Kido A, Yamamoto A, Takeuchi M, Miyaji Y, Moriya T, Sone T (2021) Comparison of biparametric and multiparametric MRI for clinically significant prostate cancer detection with PI-RADS version 2.1. J Magn Reson Imaging 53:283–291
29. Akisik FM, Sandrasegaran K, Aisen AM, Lin C, Lall C (2007) Abdominal MR imaging at 3.0 T. Radiographics 27:1433–1444
30. Lee VS, Hecht EM, Taouli B, Chen Q, Prince K, Oesingmann N (2007) Body and cardiovascular MR imaging at 3.0 T. Radiology 244:692–705
31. Schmidt C, Hötker AM, Muehlematter UJ, Burger IA, Donati OF, Barth BK (2021) Value of bowel preparation techniques for prostate MRI: a preliminary study. Abdom Radiol (NY). https://doi.org/10.1007/s00261-021-03046-3
32. Brennan DL, Lazarakis S, Lee A, Tan TH, Chin KY, Oon SF (2021) Do antispasmodics or rectal enemas improve image quality on multiparametric prostate MRI? An "Evidence-Based Practice" review of the literature Abdom Radiol (NY). https://doi.org/10.1007/s00261-020-02916-6
33. Alsop DC (1997) Phase insensitive preparation of single-shot RARE: application to diffusion imaging in humans. Magn Reson Med 38:527–533
34. Schick F (1997) SPLICE: sub-second diffusion-sensitive MR imaging using a modified fast spin-echo acquisition mode. Magn Reson Med 38:638–644
35. Feinberg DA, Hoenninger JC, Crooks LE, Kaufman L, Watts JC, Arakawa M (1985) Inner volume MR imaging: technical concepts and their application. Radiology 156:743–747
36. Tamada T, Ream JM, Doshi AM, Taneja SS, Rosenkrantz AB (2017) Reduced field-of-view diffusion-weighted magnetic resonance imaging of the prostate at 3 tesla: comparison with standard echo-planar imaging technique for image quality and tumor assessment. J Comput Assist Tomogr 41:949–956
37. Rosenkrantz AB, Chandarana H, Pfeuffer J, Triolo MJ, Shaikh MB, Mossa DJ, Geppert C (2015) Zoomed echo-planar imaging using parallel transmission: impact on image quality of diffusion-weighted imaging of the prostate at 3T. Abdom Imaging 40:120–126
38. Nelles M, König RS, Gieseke J, Guerand-van Battum MM, Kukuk GM, Schild HH, Willinek WA (2010) Dual-source parallel RF transmission for clinical MR imaging of the spine at 3.0 T: intraindividual comparison with conventional single-source transmission. Radiology 257:743–753
39. Willinek WA, Gieseke J, Kukuk GM, Nelles M, König R, Morakkabati-Spitz N, Träber F, Thomas D, Kuhl, (2010) Dual-source parallel radiofrequency excitation body MR imaging compared with standard MR imaging at 3.0 T: initial clinical experience. Radiology 256:966–975
40. Attenberger UI, Rathmann N, Sertdemir M, Riffel P, Weidner A, Kannengiesser S, Morelli JN, Schoenberg SO, Hausmann D (2016) Small Field-of-view single-shot EPI-DWI of the prostate: evaluation of spatially-tailored two-dimensional radiofrequency excitation pulses. Z Med Phys 26:168–176
41. Thierfelder KM, Scherr MK, Notohamiprodjo M, Weiß J, Dietrich O, Mueller-Lisse UG, Pfeuffer J, Nikolaou K, Theisen D (2014) Diffusion-weighted MRI of the prostate: advantages of zoomed EPI with parallel-transmit-accelerated 2D-selective excitation imaging. Eur Radiol 24:3233–3241
42. Barth BK, Cornelius A, Nanz D, Eberli D, Donati OF (2015) Diffusion-weighted imaging of the prostate: image quality and geometric distortion of readout-segmented versus selective-excitation accelerated acquisitions. Invest Radiol 50:785–791
43. Korn N, Kurhanewicz J, Banerjee S, Starobinets O, Saritas E, Noworolski S (2015) Reduced-FOV excitation decreases susceptibility artifact in diffusion-weighted MRI with endorectal coil for prostate cancer detection. Magn Reson Imaging 33:56–62
44. Brendle C, Martirosian P, Schwenzer NF, Kaufmann S, Kruck S, Kramer U, Notohamiprodjo M, Nikolaou K, Schraml C (2016) Diffusion-weighted imaging in the assessment of prostate cancer: comparison of zoomed imaging and conventional technique. Eur J Radiol 85:893–900
45. Hausmann D, Aksöz N, von Hardenberg J, Martini T, Westhoff N, Buettner S, Schoenberg SO, Riffel P (2018) Prostate cancer detection among readers with different degree of experience using ultra-high *b*-value diffusion-weighted Imaging: Is a non-contrast protocol sufficient to detect significant cancer? Eur Radiol 28:869–876
46. Mazaheri Y, Vargas HA, Nyman G, Akin O, Hricak H (2013) Image artifacts on prostate diffusion-weighted magnetic resonance imaging: trade-offs at 1.5 Tesla and 3.0 Tesla. Acad Radiol 20:1041–1047
47. Scheenen TW, Rosenkrantz AB, Haider MA, Fütterer JJ (2015) Multiparametric magnetic resonance imaging in prostate cancer management: current status and future perspectives. Invest Radiol 50:594–600
48. Gibbs P, Pickles MD, Turnbull LW (2007) Repeatability of echo-planar-based diffusion measurements of the human prostate at 3 T. Magn Reson Imaging 25:1423–1429
49. Pruessmann KP, Weiger M, Scheidegger MB, Boesiger P (1999) SENSE: Sensitivity encoding for fast MRI. Magn Reson Med 42:952–962
50. Griswold MA, Jakob PM, Heidemann RM, Nittka M, Jellus V, Wang J, Kiefer B, Haase A (2002) Generalized autocalibrating partially parallel acquisitions (GRAPPA). Magn Reson Med 47:1202–1210
51. Jeong HK, Gore JC, Anderson AW (2013) High-resolution human diffusion tensor imaging using 2-D navigated multishot SENSE EPI at 7 T. Magn Reson Med 69:793–802
52. Dai E, Zhang Z, Ma X, Dong Z, Li X, Xiong Y, Yuan C, Guo H (2018) The effects of navigator distortion and noise level on interleaved EPI DWI reconstruction: a comparison between image- and k-space-based method. Magn Reson Med 80:2024–2032
53. Otikovs M, Nissan N, Furman-Haran E, Anaby D, Allweis TM, Agassi R, Sklair-Levy M, Frydman L (2020) Diffusivity in breast malignancies analyzed for $b > 1000$ s/mm 2 at 1 mm in-plane resolutions: Insight from Gaussian and non-Gaussian behaviors. J Magn Reson Imaging 53:1913–1925
54. Baxter GC, Patterson AJ, Woitek R, Allajbeu I, Graves MJ, Gilbert F (2021) Improving the image quality of DWI in breast cancer: comparison of multi-shot DWI using multiplexed sensitivity encoding to conventional single-shot echo-planar imaging DWI. Br J Radiol 94:20200427
55. Klingebiel M, Ullrich T, Quentin M, Bonekamp D, Aissa J, Mally D, Arsov C, Albers P, Antoch G, Schimmöller L (2020) Advanced diffusion weighted imaging of the prostate: comparison of readout-segmented multi-shot, parallel-transmit and single-shot echo-planar imaging. Eur J Radiol 130:109161
56. Ueno YR, Tamada T, Takahashi S, Tanaka U, Sofue K, Kanda T, Nogami M, Ohno Y, Hinata N, Fujisawa M, Murakami T (2018) Computed diffusion-weighted imaging in prostate cancer: basics, advantages, cautions, and future prospects. Korean J Radiol 19:832–837

57. Rosenkrantz AB, Parikh N, Kierans AS, Kong MX, Babb JS, Taneja SS, Ream JM (2016) Prostate cancer detection using computed very high *b*-value diffusion-weighted imaging: How high should we go? Acad Radiol 23:704–711
58. Jendoubi S, Wagner M, Montagne S, Ezziane M, Mespoulet J, Comperat E, Estellat C, Baptiste A, Renard-Penna R (2019) MRI for prostate cancer: can computed high *b*-value DWI replace native acquisitions? Eur Radiol 29:5197–5204
59. Vural M, Ertaş G, Onay A, Acar Ö, Esen T, Sağlıcan Y, Zengingönül HP, Akpek S (2014) Conspicuity of peripheral zone prostate cancer on computed diffusion-weighted imaging: comparison of cDWI1500, cDWI2000, and cDWI3000. Biomed Res Int 2014:768291
60. Zhang K, Shen Y, Zhang X, Ma L, Wang H, An N, Guo A, Ye H (2016) Predicting prostate biopsy outcomes: a preliminary investigation on screening with ultrahigh *b*-value diffusion-weighted imaging as an innovative diagnostic biomarker. PLoS One 11:e0151176
61. Sonn GA, Margolis DJ, Marks LS (2014) Target detection: magnetic resonance imaging-ultrasound fusion-guided prostate biopsy. Urol Oncol 32:903–911
62. Rajinikanth A, Manoharan M, Soloway CT, Civantos FJ, Soloway MS (2008) Trends in Gleason score: concordance between biopsy and prostatectomy over 15 years. Urology 72:177–182
63. Le Bihan D (2013) Apparent diffusion coefficient and beyond: what diffusion MR imaging can tell us about tissue structure. Radiology 268:318–322
64. Hectors SJ, Semaan S, Song C, Lewis S, Haines GK, Tewari A, Rastinehad AR, Taouli B (2018) Advanced diffusion-weighted imaging modeling for prostate cancer characterization: correlation with quantitative histopathologic tumor tissue composition-a hypothesis-generating study. Radiology 286:918–928
65. Hoeks CM, Barentsz JO, Hambrock T, Yakar D, Somford DM, Heijmink SW, Scheenen TW, Vos PC, Huisman H, van Oort IM, Witjes JA, Heerschap A, Fütterer JJ (2011) Prostate cancer: multiparametric MR imaging for detection, localization, and staging. Radiology 261:46–66
66. Turkbey B, Shah VP, Pang Y et al (2011) Is apparent diffusion coefficient associated with clinical risk scores for prostate cancers that are visible on 3-T MR images? Radiology 258(2):488–495
67. Hambrock T, Somford DM, Huisman HJ, van Oort IM, Witjes JA, Hulsbergen-van de Kaa CA, Scheenen T, Barentsz JO (2011) Relationship between apparent diffusion coefficients at 3.0-T MR imaging and Gleason grade in peripheral zone prostate cancer. Radiology 259:453–461
68. Doo KW, Sung DJ, Park BJ, Kim MJ, Cho SB, Oh YW, Ko YH, Yang KS (2012) Detectability of low and intermediate or high risk prostate cancer with combined T2-weighted and diffusion-weighted MRI. Eur Radiol 22:1812–1819
69. Tamada T, Kanomata N, Sone T, Jo Y, Miyaji Y, Higashi H, Yamamoto A, Ito K (2014) High *b* value (2,000 s/mm^2) diffusion-weighted magnetic resonance imaging in prostate cancer at 3 Tesla: comparison with 1000 s/mm^2 for tumor conspicuity and discrimination of aggressiveness. PLoS One 9:e96619
70. Barbieri S, Brönnimann M, Boxler S, Vermathen P, Thoeny HC (2017) Differentiation of prostate cancer lesions with high and with low gleason score by diffusion-weighted MRI. Eur Radiol 27:1547–1555
71. Donati OF, Mazaheri Y, Afaq A, Vargas HA, Zheng J, Moskowitz CS, Hricak H, Akin O (2014) Prostate cancer aggressiveness: assessment with whole-lesion histogram analysis of the apparent diffusion coefficient. Radiology 271:143–152
72. Lu ZH, Ji LB, Zhao WL, Zhang YS, Wu JF, Li X, Shen JK (2019) Differentiating transition zone cancers from benign prostatic hyperplasia by histogram analysis of apparent diffusion coefficient maps with standard and ultrahigh *b*-value diffusion-weighted MR Imaging. J Comput Assist Tomogr 43:235–241
73. Rosenkrantz AB, Ream JM, Nolan P, Rusinek H, Deng FM, Taneja SS (2015) Prostate cancer: utility of whole-lesion apparent diffusion coefficient metrics for prediction of biochemical recurrence after radical prostatectomy. AJR Am J Roentgenol 205:1208–1214
74. Tamada T, Prabhu V, Li J, Babb JS, Taneja SS, Rosenkrantz AB (2017) Prostate cancer: diffusion-weighted MR imaging for detection and assessment of aggressiveness-comparison between conventional and kurtosis models. Radiology 284:100–108
75. Rosenkrantz AB, Padhani AR, Chenevert TL, Koh DM, De Keyzer F, Taouli B, Le Bihan D (2015) Body diffusion kurtosis imaging: basic principles, applications, and considerations for clinical practice. J Magn Reson Imaging 42:1190–1202
76. Le Bihan D, Breton E, Lallemand D, Grenier P, Cabanis E, Laval-Jeantet M (1986) MR imaging of intravoxel incoherent motions: application to diffusion and perfusion in neurologic disorders. Radiology 161:401–407
77. Le Bihan D, Breton E, Lallemand D, Aubin ML, Vignaud J, Laval-Jeantet M (1988) Separation of diffusion and perfusion in intravoxel incoherent motion MR imaging. Radiology 168:497–505
78. Toivonen J, Merisaari H, Pesola M, Taimen P, Boström PJ, Pahikkala T, Aronen HJ, Jambor I (2015) Mathematical models for diffusion-weighted imaging of prostate cancer using b-values up to 2000 s/mm(2): correlation with Gleason score and repeatability of region of interest analysis. Magn Reson Med 74:1116–1124
79. Bao J, Wang X, Hu C, Hou J, Dong F, Guo L (2017) Differentiation of prostate cancer lesions in the Transition Zone by diffusion-weighted MRI. Eur J Radiol Open 4:123–128
80. Shan Y, Chen X, Liu K, Zeng M, Zhou J (2019) Prostate cancer aggressive prediction: preponderant diagnostic performances of intravoxel incoherent motion (IVIM) imaging and diffusion kurtosis imaging (DKI) beyond ADC at 3.0 T scanner with gleason score at final pathology. Abdom Radiol (NY) 44:3441–3452
81. Yang DM, Kim HC, Kim SW, Jahng GH, Won KY, Lim SJ, Oh JH (2016) Prostate cancer: correlation of intravoxel incoherent motion MR parameters with Gleason score. Clin Imaging 40:445–450
82. Merisaari H, Movahedi P, Perez IM, Toivonen J, Pesola M, Taimen P, Boström PJ, Pahikkala T, Kiviniemi A, Aronen HJ, Jambor I (2017) Fitting methods for intravoxel incoherent motion imaging of prostate cancer on region of interest level: repeatability and gleason score prediction. Magn Reson Med 77:1249–1264
83. Valerio M, Zini C, Fierro D, Giura F, Colarieti A, Giuliani A, Laghi A, Catalano C, Panebianco V (2016) 3T multiparametric MRI of the prostate: Does intravoxel incoherentmotion diffusion imaging have a role in the detection andstratification of prostate cancer in the peripheral zone? Eur J Radiol 85:790–794
84. Liu Y, Wang X, Cui Y, Jiang Y, Yu L, Liu M, Zhang W, Shi K, Zhang J, Zhang C, Li C, Chen M (2020) Comparative study of monoexponential, intravoxel incoherent motion, kurtosis, and IVIM-kurtosis models for the diagnosis and aggressiveness assessment of prostate cancer. Front Oncol 10:1763
85. Zhang YD, Wang Q, Wu CJ, Wang XN, Zhang J, Liu H, Liu XS, Shi HB (2015) The histogram analysis of diffusion-weighted intravoxel incoherent motion (IVIM) imaging for differentiating the gleason grade of prostate cancer. Eur Radiol 25:994–1004
86. Liu W, Liu XH, Tang W, Gao HB, Zhou BN, Zhou LP (2018) Histogram analysis of stretched-exponential and monoexponential diffusion-weighted imaging models for distinguishing low and intermediate/high gleason scores in prostate carcinoma. J Magn Reson Imaging 48:491–498

87. Kim E, Kim CK, Kim HS, Jang DP, Kim IY, Hwang J (2020) Histogram analysis from stretched exponential model on diffusion-weighted imaging: evaluation of clinically significant prostate cancer. Br J Radiol 935:20190757
88. Suo S, Chen X, Wu L, Zhang X, Yao Q, Fan Y, Wang H, Xu J (2014) Non-Gaussian water diffusion kurtosis imaging of prostate cancer. Magn Reson Imaging 32:421–427
89. Rosenkrantz AB, Sigmund EE, Johnson G, Babb JS, Mussi TC, Melamed J, Taneja SS, Lee VS, Jensen JH (2012) Prostate cancer: feasibility and preliminary experience of a diffusional kurtosis model for detection and assessment of aggressiveness of peripheral zone cancer. Radiology 264:126–135
90. Wang Q, Li H, Yan X et al (2015) Histogram analysis of diffusion kurtosis magnetic resonance imaging in differentiation of pathologic Gleason grade of prostate cancer. Urol Oncol 33(8):337.e15–24
91. Roethke MC, Kuder TA, Kuru TH et al (2015) Evaluation of diffusion kurtosis imaging versus standard diffusion imaging for detection and grading of peripheral zone prostate cancer. Invest Radiol 50(8):483–489
92. Park H, Kim SH, Lee Y, Son JH (2020) Comparison of diagnostic performance between diffusion kurtosis imaging parameters and mono-exponential ADC for determination of clinically significant cancer in patients with prostate cancer. Abdom Radiol (NY) 45:4235–4243
93. Wang X, Tu N, Qin T, Xing F, Wang P, Wu G (2018) Diffusion Kurtosis Imaging combined with DWI at 3-T MRI for detection and assessment of aggressiveness of prostate cancer. AJR Am J Roentgenol 211:797–804]
94. Damascelli A, Gallivanone F, Cristel G, Cava C, Interlenghi M, Esposito A, Brembilla G, Briganti A, Montorsi F, Castiglioni I, De Cobelli F (2021) Advanced imaging analysis in prostate MRI: building a radiomic signature to predict tumor aggressiveness. Diagnostics (Basel) 11:594
95. Chen T, Li M, Gu Y, Zhang Y, Yang S, Wei C, Wu J, Li X, Zhao W, Shen J. Prostate Cancer Differentiation and Aggressiveness: Assessment With a Radiomic-Based Model vs. PI-RADS v2. J Magn Reson Imaging 49:875–884
96. Xu L, Zhang G, Zhao L, Mao L, Li X, Yan W, Xiao Y, Lei J, Sun H, Jin Z (2020) Radiomics based on multiparametric magnetic resonance imaging to predict extraprostatic extension of prostate cancer. Front Oncol 16(10):940
97. Siddiqui MM, Rais-Bahrami S, Turkbey B, George AK, Rothwax J, Shakir N, Okoro C, Raskolnikov D, Parnes HL, Linehan WM, Merino MJ, Simon RM, Choyke PL, Wood BJ, Pinto PA (2015) Comparison of MR/ultrasound fusion-guided biopsy with ultrasound-guided biopsy for the diagnosis of prostate cancer. JAMA 27(313):390–397
98. Rouvière O, Puech P, Renard-Penna R, Claudon M, Roy C, Mège-Lechevallier F, Decaussin-Petrucci M, Dubreuil-Chambardel M, Magaud L, Remontet L, Ruffion A, Colombel M, Crouzet S, Schott AM, Lemaitre L, Rabilloud M, Grenier N, Investigators MRI-FIRST (2019) Use of prostate systematic and targeted biopsy on the basis of multiparametric MRI in biopsy-naive patients (MRI-FIRST): a prospective, multicentre, paired diagnostic study. Lancet Oncol 20:100–109
99. Borofsky S, George AK, Gaur S, Bernardo M, Greer MD, Mertan FV, Taffel M, Moreno V, Merino MJ, Wood BJ, Pinto PA, Choyke PL, Turkbey B (2018) What are we missing? False-negative cancers at multiparametric MR imaging of the prostate. Radiology 286:186–195
100. Kido A, Tamada T, Kanomata N, Yamamoto A, Miyaji Y, Nagai A, Sone T (2019) Multidimensional analysis of clinicopathological characteristics of false-negative clinically significant prostate cancers on multiparametric MRI of the prostate in Japanese men. Jpn J Radiol 37:154–164
101. Chatterjee A, Watson G, Myint E, Sved P, McEntee M, Bourne R (2015) Changes in epithelium, stroma, and lumen space correlate more strongly with gleason pattern and are stronger predictors of prostate adc changes than cellularity metrics. Radiology 277:751–762
102. Chatterjee A, Harmath C, Oto A (2020) New prostate MRI techniques and sequences. Abdom Radiol (NY) 45:4052–4062
103. Wu D, Jiang K, Hsu YC, Sun Y, Zhang Y, Zhang Y (2021) Microstructural mapping with diff usion-time dependent diff usion MRI improves diagnosis ofprostate cancer at 3T. Proceedings of the 2021 Annual Meeting of ISMRM, 0695.
104. White NS, Leergaard TB, D'Arceuil H, Bjaalie JG, Dale AM (2013) Probing tissue microstructure with restriction spectrum imaging: histological and theoretical validation. Hum Brain Mapp 34:327–346
105. White NS, McDonald C, Farid N, Kuperman J, Karow D, Schenker-Ahmed NM, Bartsch H, Rakow-Penner R, Holland D, Shabaik A, Bjørnerud A, Hope T, Hattangadi-Gluth J, Liss M, Parsons JK, Chen CC, Raman S, Margolis D, Reiter RE, Marks L, Kesari S, Mundt AJ, Kane CJ, Carter BS, Bradley WG, Dale AM (2014) Diffusion-weighted imaging in cancer: physical foundations and applications of restriction spectrum imaging. Can Res 74:4638–4652
106. McCammack KC, Kane CJ, Parsons JK, White NS, Schenker-Ahmed NM, Kuperman JM, Bartsch H, Desikan RS, Rakow-Penner RA, Adams D, Liss MA, Mattrey RF, Bradley WG, Margolis DJ, Raman SS, Shabaik A, Dale AM, Karow DS (2016) In vivo prostate cancer detection and grading using restriction spectrum imaging-MRI. Prostate Cancer Prostatic Dis 19:168–173
107. Felker ER, Raman SS, Shakeri S, Mirak SA, Bajgiran AM, Kwan L, Khoshnoodi P, ElKhoury FF, Margolis DJA, Karow D, Lu DSK, White N, Marks LS (2019) Utility of restriction spectrum imaging among men undergoing first-time biopsy for suspected prostate cancer. AJR Am J Roentgenol 213:365–370
108. Tamada T, Kido A, Takeuchi M, Yamamoto A, Miyaji Y, Kanomata N, Sone T (2019) Comparison of PI-RADS version 2 and PI-RADS version 2.1 for the detection of transition zone prostate cancer. Eur J Radiol 121:108704
109. Panagiotaki E, Walker-Samuel S, Siow B, Johnson SP, Rajkumar V, Pedley RB, Lythgoe MF, Alexander DC (2014) Noninvasive quantification of solid tumor microstructure using VERDICT MRI. Cancer Res 74:1902–1912
110. Johnston EW, Bonet-Carne E, Ferizi U, Yvernault B, Pye H, Patel D, Clemente J, Piga W, Heavey S, Sidhu HS, Giganti F, O'Callaghan J, Brizmohun Appayya M, Grey A, Saborowska A, Ourselin S, Hawkes D, Moore CM, Emberton M, Ahmed HU, Whitaker H, Rodriguez-Justo M, Freeman A, Atkinson D, Alexander D, Panagiotaki E, Punwani S (2019) VERDICT MRI for prostate cancer: intracellular volume fraction versus apparent diffusion coefficient. Radiology 291:391–397
111. Chatterjee A, Bourne RM, Wang S, Devaraj A, Gallan AJ, Antic T, Karczmar GS, Oto A (2018) Diagnosis of prostate cancer with noninvasive estimation of prostate tissue composition by using hybrid multidimensional MR imaging: a feasibility study. Radiology 287:864–873
112. Sadinski M, Karczmar G, Peng Y, Wang S, Jiang Y, Medved M, Yousuf A, Antic T, Oto A (2016) Pilot study of the use of hybrid multidimensional T2-weighted imaging-DWI for the diagnosis of prostate cancer and evaluation of gleason score. AJR Am J Roentgenol 207:592–598
113. Wang S, Peng Y, Medved M, Yousuf AN, Ivancevic MK, Karademir I, Jiang Y, Antic T, Sammet S, Oto A, Karczmar GS (2014) Hybrid multidimensional T(2) and diffusion-weighted MRI for prostate cancer detection. J Magn Reson Imaging 39:781–788